

Supporting Information

Gas-phase Structures Reflect Pain-relief Potency of Enkephalin Peptides.

Aleksandr Y. Pereverzev,¹ István Szabó,² Vladimir N. Kopysov¹, Edina Rosta², and
Oleg V. Boyarkin^{1*}

¹Laboratoire de Chimie Physique Moléculaire, École Polytechnique Fédérale de Lausanne, Station-6, 1015 Lausanne, Switzerland.

²Department of Chemistry, King's College London, Britannia House, 7 Trinity Street, London SE1 1DB, United Kingdom.

Table of Contents

Experimental	S2
Computational details.....	S3
Figure S1. UV and IR-UV spectra of DL	S5
Table S1. Relative energies of <i>DD</i> structures.....	S6
Figure S2. IR spectra of the lead and non-compact structures of <i>DD</i>	S7
Figure S3. Clustering of <i>DL</i> structures.....	S8
Table S2. Relative energies of <i>DL</i> structures	S9
Figure S4. IR spectra of the lead structures of <i>DL</i>	S10
Figure S5. Calculated lowest-energy <i>LL</i> structure and its IR spectrum.....	S11
Table S3. Gas-phase pharmacological parameters in enkephalins.....	S12
Figure S6. IR-UV hole-burning spectra of <i>DD</i>	S13
Figure S7. FRET data for <i>DL</i>	S14
Figure S8. Selected calculated IR spectra of <i>DL</i> and the experimental one of <i>DL-A</i>	S15
Figure S9. IR-UV gain spectrum of <i>DL</i> measured at different ion source conditions....	S16
Additional references	S16

* Corresponding Author: oleg.boiarin@epfl.ch

1. Experimental

Protonated gas-phase ions are produced from solution using a nanoelectrospray ion source (Proxeon), and enter into a two-stage electrodynamic ion funnel²⁰ (Spectrograph) through 0.7 mm ID, 10 cm long metal capillary, orthogonally to the funnel axis. The funnel guides the ions into a home-made hexapole RF trap, where they are accumulated and thermalized for approximately 100 ms. The ions are then released from the trap and mass-selected by a quadrupole mass filter (Extrel), bent 90° by an electrostatic quadrupole bender, decelerated by a stack of electrostatic lenses and, finally, guided by an octupole ion guide into a cold octupole ion trap. The trap is mounted on a cold head (T=6 K) of a two-stage closed cycle refrigerator (RDS-407, Sumitomo). The ions are trapped and cooled in the octupole to T=10 K by collisions with He gas, which we pulse into the trap right before the arrival of the ion packet.¹⁸ A UV and two IR laser beams counterpropagate into the vacuum chamber through two BaF₂ windows 100 μs before the release of the parent and UV-induced fragment ions from the trap. The beams are spatially overlapped on the axis of the trap. Laser pulses are separated by 200 ns time delays. The released ions are 90° bent by the second electrostatic quadrupole bender and analyzed in a quadrupole mass spectrometer (Extrel), equipped with a channeltron ion detector. Ion signals from the channeltron are, finally, counted by a gated photon counter (SR400, SRS Inc.), which transfers the data to a host PC, which controls the data acquisition via LabView software. We fill the cold trap in 10 Hz cycles, running the UV laser and the probe IR OPO at the same repetition rate, while the pump IR fires at 5 Hz in every second cycle. We typically take an average of 20 laser shots per data point in spectral measurements. Firing of the UV laser and the two IR OPOs, the release of ions from the hexapole and from the cold octupole traps, and the data acquisition system are synchronized using three multichannel pulse generators (BNC 575). UV light is produced by frequency doubling the output of a dye laser (HD-500, Lumonics) in a KDP crystal. The dye laser is pumped by 150 mJ of the 3rd harmonic of a Nd:YAG laser (GCR-210, Spectra-Physics). The beam is loosely focused by F=70 cm fused silica lens 2-3 cm in front of the cold trap entrance. IR beams are generated by two tunable optical parametric oscillator (OPO) (Laser Vision), pumped by two different Nd:YAG lasers (Surelite III-Ex, Continuum; SpitLight 600, Innolas). The beams are focused to the center of the trap by two F=70 cm CaF₂ lenses. Spectral resolution of the IR OPO is about 1 cm⁻¹ in the 3 μm region and around 2 cm⁻¹ in the 6 μm.

UV spectra allow for evaluation of the overall resemblance of the isomers and reveal the transitions suitable for their IR spectroscopy. In IR-UV hole-burning spectra the vibronic transitions of the conformers that are preheated by a preceding IR laser pulse are (strongly) suppressed, which allows for conformational assignment of these transitions (e.g., Fig 3). An IR-UV gain spectrum reflects vibrational transitions in all abundant conformers of an ion (e.g., Fig. 1a). IR-UV depletion provides vibrational spectra of the conformers, labelled by their resolved UV transitions (e.g., Fig. 4b). Whenever UV transitions are not resolved and the depletion spectroscopy is challenging, IR-IR-UV hole-burning enables conformer-selective vibrational spectroscopy by employing the resolved in a gain spectrum IR peaks as tags for conformers. The IR spectrum of a conformer that is preheated by the first pump IR OPO is obtained by subtracting the measured triple resonance trace (IR-IR-UV) from the gain one (IR-UV) measured in two alternative cycles. This results in an IR spectrum of the conformer that was pre-heated by the first IR OPO (e.g., Figs. 1b-c).

All peptides of >95% purity were purchased from Sigma-Aldrich and used without further purification. Sample solutions with the final concentration of 50 μ M were prepared in HPLC grade solvents to water/methanol/acetic acid 100:100:1 (V/V/V) mixture.

2. Computational details

Our computational methodology consists of the following steps:

- (1) finding all possible geometries using classical force field-based methods;
- (2) clustering of the geometries based on the RMSD of coordinates of all heavy atoms (Figs. S1 and S3);
- (3) finding lowest-energy lead structures in each cluster with a multistep low-to-high level DFT-based geometry optimization;
- (4) identification of the candidate clusters by comparing the experimental IR spectra with the computed ones for all lead structures (Figs. S2 and S4);
- (5) finding the best-matching structure in the cluster.

In step 1 we employ the Monte Carlo Multiple Minimum method combined with the low-mode conformation search algorithm^{32,33} as implemented in the Macromodel plugin of the Schrödinger Suit. The *DL* and *DD* conformations are exhaustively generated using the OPLS3 force-field. Redundant conformers are eliminated by setting the maximum

atom deviation to 0.5 Å. The chirality of amino acid residues is maintained during the conformational search. In total 146, and 174 conformers were extracted for the *DD* and *DL* stereoisomers, respectively. Subsequently, conformational clustering is applied, which considers the RMSD of all the heavy atoms.

Followed by the visual inspection of the lowest energy structures in each cluster, the correct lead structures are identified in step 3 by more rigorous DFT geometry optimizations in gas phase using the hybrid B3LYP exchange-correlation functional in combination with the 6-31G* basis-set, referred to as low-level of theory. All the visually detected occasional “non-standard” structures in each cluster were moved out to an additional cluster and re-examined at the same level of theory. The low-level DFT optimizations are performed in each cluster obtained in the force-field screening up to 6 kcal mol⁻¹. Then, all the geometries in the 0-6 kcal mol⁻¹ energy window of the low-level optimized structures are re-optimized using the same B3LYP functional employing the larger 6-31+G** basis-set. The later method and basis set combination is referred to as high-level of theory. Grimme’s D3 dispersion correction is included in all computations.^{34,35} For the accurate description of the low frequency modes an ultrafine DFT integration grid and tight convergence is requested. No symmetry restrictions are imposed during the geometry optimization procedure.

Subsequently, the harmonic vibrational frequencies are generated at the B3LYP/6-31+G** with GD3 level, corresponding to the equilibrium structures obtained at the high-level of theory. All the frequencies are empirically adjusted with the same scaling factor of 0.9545 and compared to the experimental spectra to choose the best candidate structures for conformers of *DD* and *DL* isomers. All standard DFT computations were performed with the Gaussian 09³⁶ *ab initio* program package.

As a test, the calculated lowest energy structure of the *LL* stereoisomer (Fig. S3) appears almost identical to the recently reported gas-phase structure of the most stable conformer of this peptide²⁰ with RMSD of the coordinates of heavy atoms in the two geometries as small as 0.00743 Å. The calculated (in a harmonic approximation, scaled) IR spectrum of this structure exhibits an excellent match to the reported²⁰ experimental spectrum of this conformer (Fig. S3a). We are thus confident that our workflow of conformational search and the accuracy of calculations are appropriate.

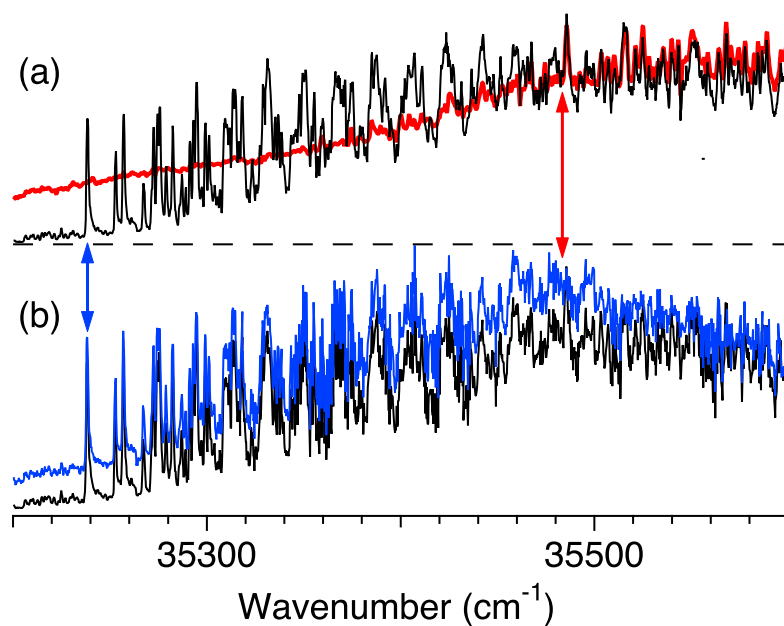


Figure S1. Electronic spectrum of *DL* (black traces), and its IR-UV hole-burning spectra recorded with IR wavenumber fixed at (a) 3411.2 and (b) 3466.5 cm^{-1} (red and blue traces, respectively). The arrows marks the electronic band origin in *DL-A* (blue) and *DL-B* (red).

Table S1. Relative energies and clustering of the *DD* geometries within 0-6 kcal/mol energy window

Structure ID	$E_{\text{rel}} / \text{kcal mol}^{-1}$	Cluster ID
75	0.00	1
39	0.03	1
54	0.06	1
25	0.08	1
59	0.23	2
66	0.27	2
106	1.11	1
42	1.13	2
47	1.29	2
126	1.37	1
80	1.40	1
110	1.42	1
56	1.42	1
57	1.45	1
88	1.52	2
104	1.60	3
92	1.66	2
97	1.89	3
72	1.93	2
62	2.18	4
138	2.24	3
132	2.37	5
101	2.51	6
107	2.52	6
127	2.76	7
64	3.56	8
34	3.83	9

Structure ID	$E_{\text{rel}} / \text{kcal mol}^{-1}$	Cluster ID
134	3.85	6
139	3.87	6
38	4.07	9
1	4.12	10
2	4.38	10
13	4.46	11
5	4.57	12
9	4.86	12
78	4.89	9
35	5.07	11
91	5.09	8
116	5.09	13
37	5.10	11
82	5.12	9
90	5.20	9
133	5.21	14
112	5.24	15
117	5.31	13
40	5.33	11
6	5.33	10
41	5.35	11
93	5.45	9
128	5.48	15
23	5.57	12
10	5.61	10
8	5.76	10
26	5.89	12

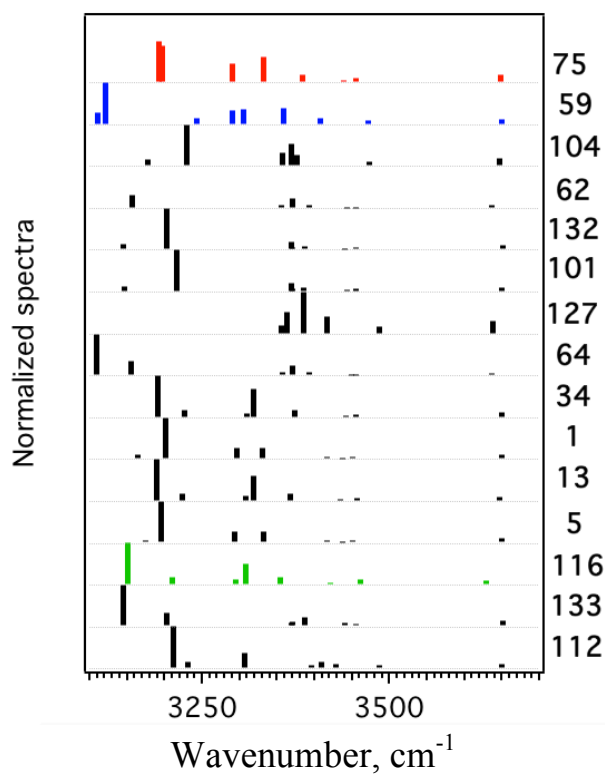


Figure S2a. Comparison of the computed IR spectra of the lead structures of clusters of *DD*. Color-coded spectra exhibit the best match with the experimental ones.

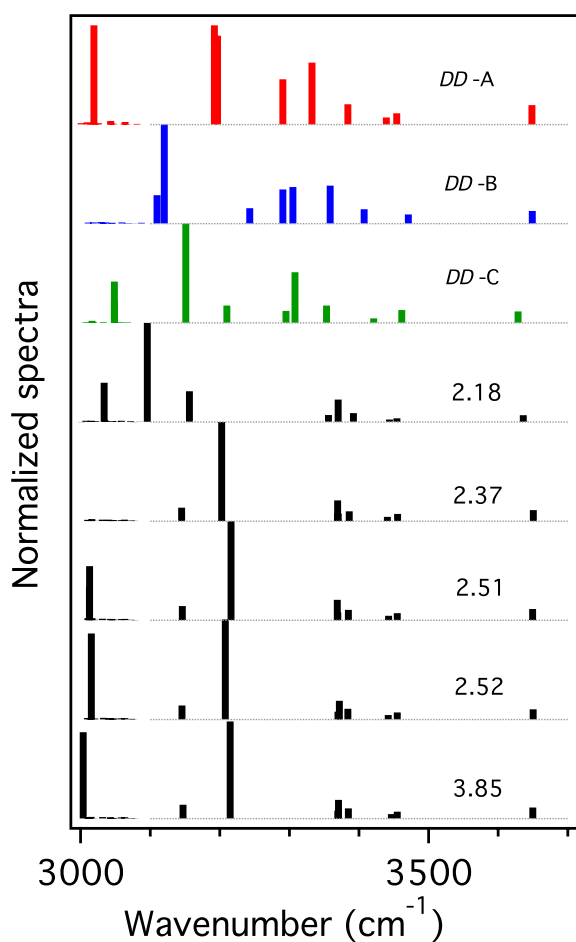


Figure S2b. Comparison of the computed IR spectra (a) of the *DD-A*, *DD-B* and *DD-C* structures, which are all compact, with the spectra of the lowest energy non-compact calculated structures (black sticks; energy is in kcal/M). The patterns of the spectra for the compact and the non-compact structures are qualitatively different.

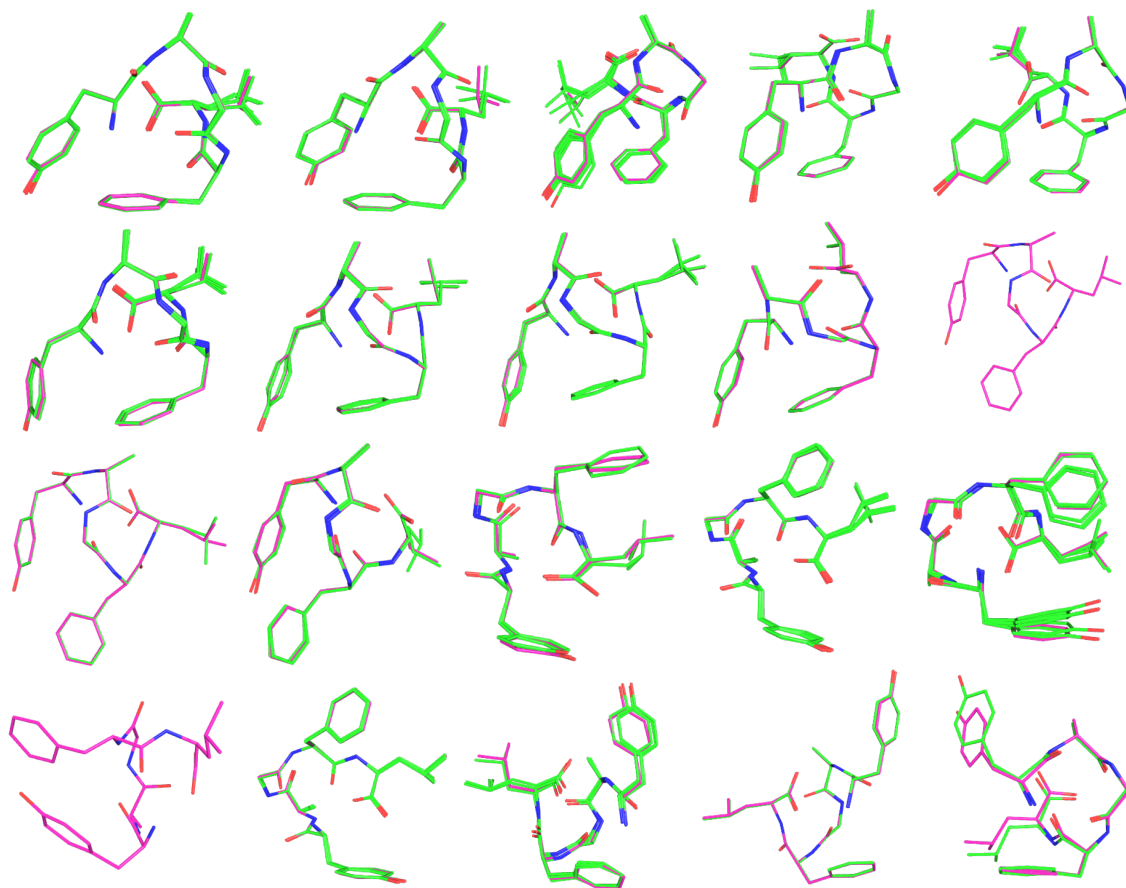


Figure S3. Clustering of the 83 structures of *DL*, whose relative energies with respect to the lowest-energy one do not exceed 6 kcal/mol. Carbon atoms of the lead structures are drawn in magenta.

Table S2. Relative energies and clustering of the *DL* geometries within 0-6 kcal/mol energy window

Structure ID	$E_{\text{rel}} / \text{kcal mol}^{-1}$	Cluster ID
5	0.00	1
13	0.11	1
35	0.14	2
8	0.73	3
34	0.80	1
46	0.91	1
14	1.02	3
75	1.17	2
51	1.28	4
71	1.31	4
37	1.32	1
80	1.34	2
101	1.41	2
56	1.41	1
28	1.78	5
29	1.84	5
7	1.93	6
9	2.05	6
39	2.14	3
96	2.24	7
58	2.39	8
82	2.53	7
108	2.57	4
134	2.57	4
160	2.63	9
173	2.63	9
50	2.66	8
36	2.87	6
63	2.88	5
127	2.88	10
38	3.03	6
85	3.08	11
40	3.12	6
73	3.18	5
44	3.24	6
78	3.25	5
112	3.27	3
42	3.36	12
120	3.41	8
124	3.44	13
119	3.62	3
158	3.66	7

Structure ID	$E_{\text{rel}} / \text{kcal mol}^{-1}$	Cluster ID
123	3.68	8
113	3.68	8
43	3.73	3
23	3.76	14
21	3.76	14
129	3.77	13
117	3.94	8
153	3.97	7
24	4.01	14
31	4.02	14
144	4.10	11
3	4.21	15
154	4.36	16
92	4.49	14
4	4.49	15
86	4.49	14
6	4.51	15
97	4.55	14
90	4.55	14
121	4.57	3
102	4.61	12
95	4.76	14
107	4.77	14
68	4.92	12
126	4.93	3
15	4.95	15
155	5.05	13
128	5.33	17
125	5.35	17
19	5.37	15
174	5.39	18
169	5.39	18
164	5.56	19
135	5.61	17
122	5.62	17
139	5.63	18
159	5.64	19
146	5.70	18
11	5.97	15
136	6.10	20
142	6.27	20

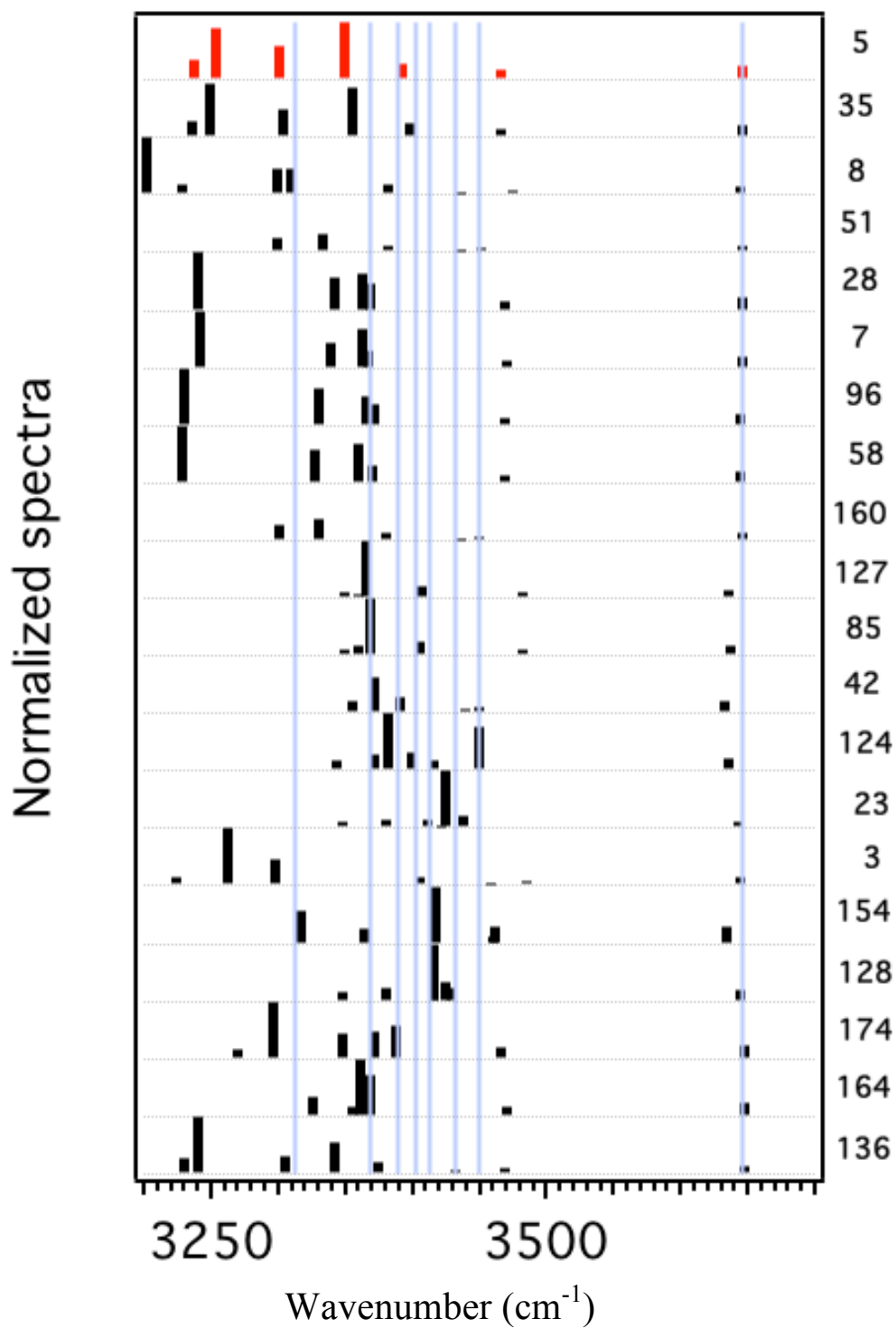


Figure S4. Comparison of the computed IR spectra of the lead structures of clusters of *DL*. Vertical blue lines correspond to IR transitions of the conformer *DL-A*.

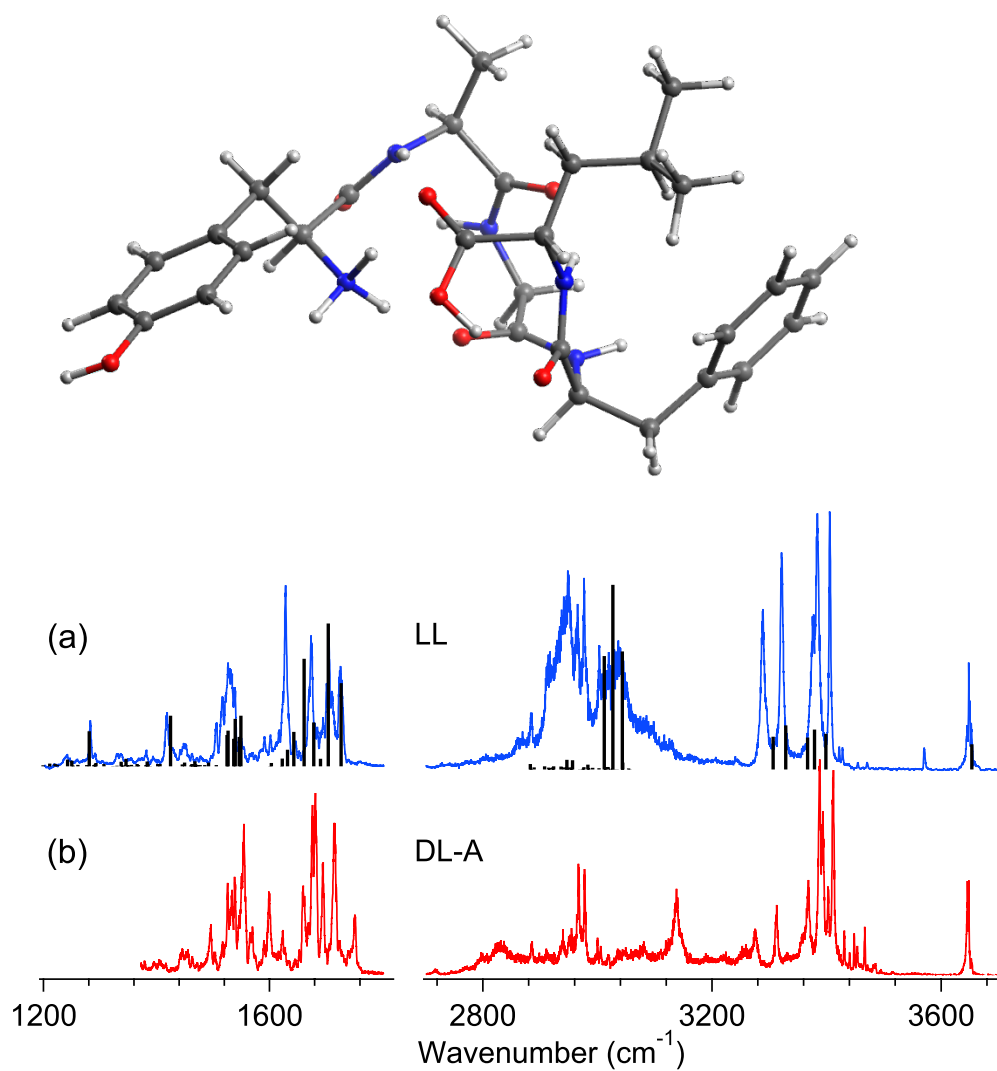


Figure S5. IR-UV spectrum of (a) *LL* isomer of Ala²-enkephalin²⁰ and (b) *DL-A* conformer of the same peptide. The black sticks in (a) show the spectrum (scaled by 0.9545 and by 0.985 for 3 and 6 μm regions, respectively) calculated for the most stable computed structure of *LL*.

Table S3. Gas-phase pharmacological parameters in enkephalins, Å

Molecule, isoform	H ₃ N–Tyr ring	H ₃ N–Phe ring	Ring–ring centers
Enkephalin			
(YGGFL), <i>LL</i>	3.8	8.2	11.6
Ala ² -enkephalin			
(YAGFL), <i>LL</i>	3.8	8.1	11.6
Ala ² -enkephalin			
(YAGFL), <i>DD-A</i>	3.7	3.0	4.7
<i>DD-B</i>	3.8	3.1	4.7
<i>DD-C</i>	3.7	3.0	4.4
Ala ² -enkephalin			
(YAGFL), <i>DL-B</i>	3.8	3.3	4.8

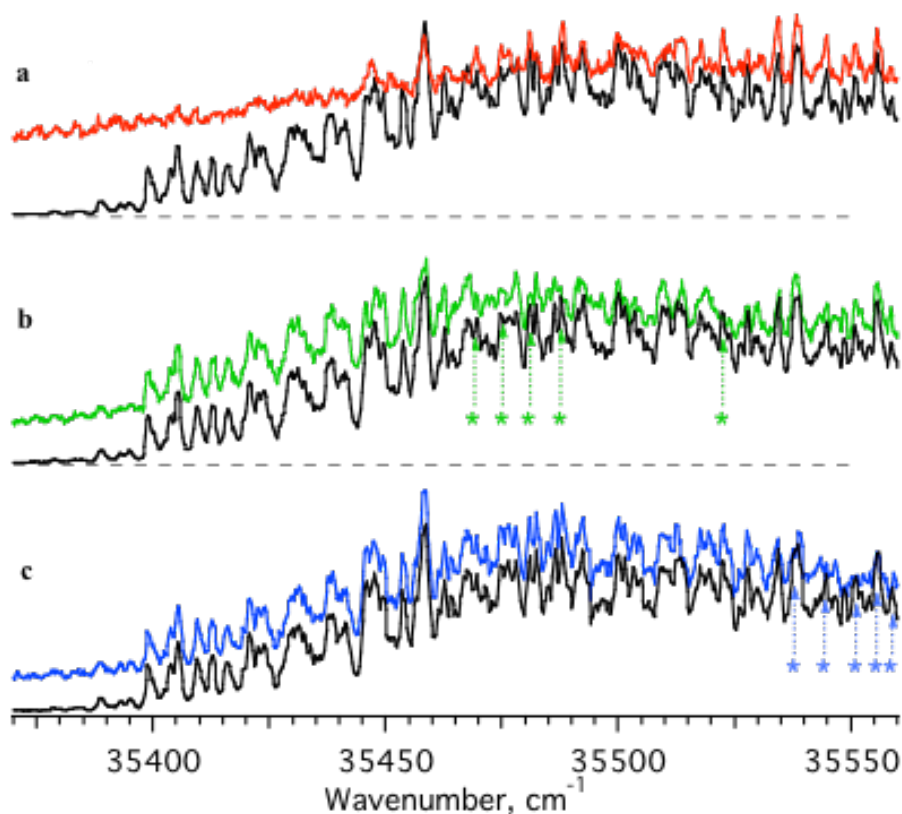


Figure S6. IR-UV hole-burning spectra of protonated *DD* isomer of Ala²-enkephalin. The black traces are the electronic spectrum of cold *DD*; the color traces are the electronic spectra of IR pre-heated *DD* with IR OPO wavenumber fixed at a) 3329.2 cm⁻¹, b) 3413 cm⁻¹, and c) 3689.1 cm⁻¹. Fixing wavenumber of the pump IR laser at these wavenumbers results in reducing UV photofragmentation yield for three different sets of electronic transitions, which therefore have been assigned to three different conformers of *DD*. Asterisks mark the detected conformer-specific electronic transitions in each conformer.

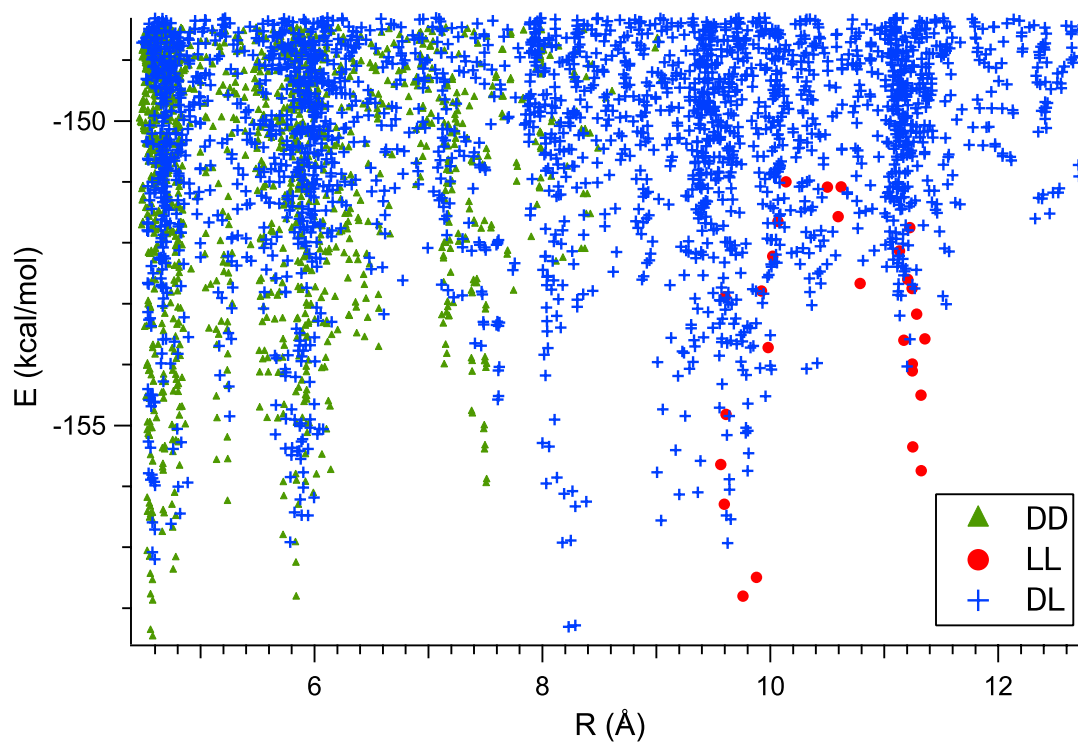


Figure S7. Potential energy as a function of the interchromophore distance of the computed (MM-level) structures for DD ,¹¹ LL ¹¹ and DL stereoisomers of protonated YAGFL enkephalins, constrained by FRET measurements (see ref. 11 for details). In contrast to DD and LL , the distribution of DL structures samples the 4 to 12 Å wide range of possible interchromophore distances.

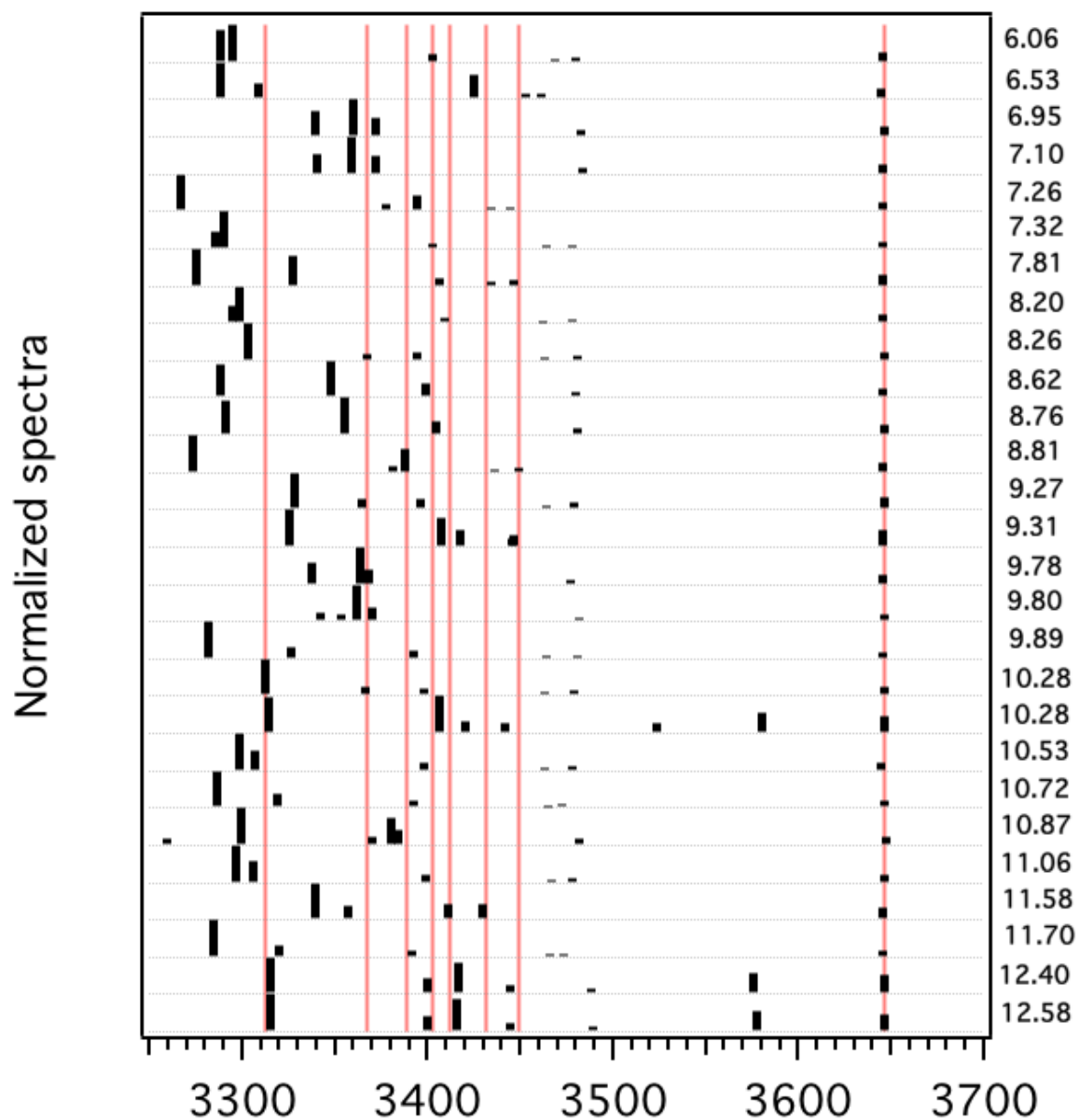


Figure S8. Selected calculated IR spectra of *DL* conformers with relative energies with respect to the lowest-energy structure (numbers on the right) lie within 6-12 kcal/mol window. Vertical red lines denote experimentally obtained transitions of the conformer *DL-A*.

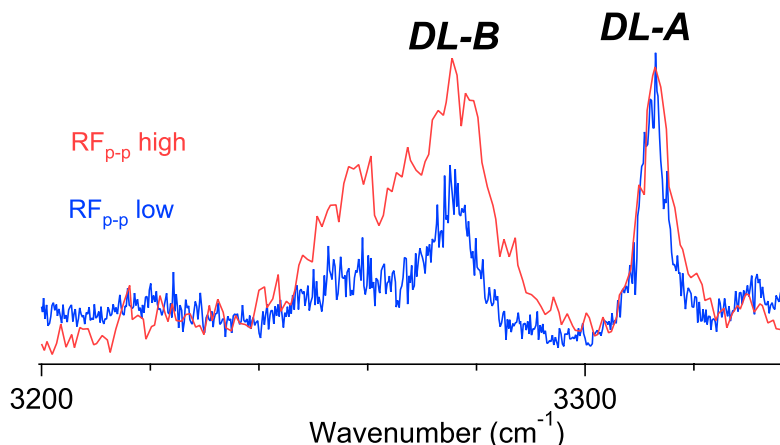


Figure S9. IR gain spectrum of *DL* stereoisomer measured at two different RF amplitudes in the ion funnel of the electrospray ion source. The spectrum was measured in the spectral region that contains peaks of comparable intensities due to both conformers. The red trace is the average of 5 scans, required due to low parent ion signal. The blue trace is reproduced from the spectrum in Fig 4a. For graphical clarity the spectra were scaled in intensity to align the peak of *DL-A*. Internal RF heating results in the decreased abundance of the higher-energy gas-phase structure *DL-A*, which is consistent with kinetic trapping of *DL-A*.

Additional references

- (32) Kolossváry, I.; Guida, W. C., *J. Am. Chem. Soc.* **1996**, 118, 5011-5019.
 (33) Kolossváry, I.; Guida, W. C., *J. Comp. Chem.* **1999**, 20, 1671-1684.
 (34) Grimme, S. *J. Comput. Chem.* **2006**, 27, 1787-1799.
 (35) Grimme, S.; Ehrlich, S.; Goerigk, L. *J. Comput. Chem.* **2011**, 32 (7), 1456–1465.
 (36) Frisch, M. J.; Trucks, G. W.; Schlegel, H. B.; Scuseria, G. E.; Robb, M. A.; Cheeseman, J. R.; Scalmani, G.; Barone, V.; Mennucci, B.; Petersson, G. A.; Nakatsuji, H.; Caricato, M.; Li, X.; Hratchian, H. P.; Izmaylov, A. F.; Bloino, J.; Zheng, G.; Sonnenberg, J. L.; Hada, M.; Ehara, M.; Toyota, K.; Fukuda, R.; Hasegawa, J.; Ishida, M.; Nakajima, T.; Honda, Y.; Kitao, O.; Nakai, H.; Vreven, T.; Montgomery Jr., J. A.; Peralta, J. E.; Ogliaro, F.; Bearpark, M.; Heyd, J. J.; Brothers, E.; Kudin, K. N.; Staroverov, V. N.; Kobayashi, R.; Normand, J.; Raghavachari, K.; Rendell, A.; Burant, J. C.; Iyengar, S. S.; Tomasi, J.; Cossi, M.; Rega, N.; Millam, J. M.; Klene, M.; Knox, J. E.; Cross, J. B.; Bakken, V.; Adamo, C.; Jaramillo, J.; Gomperts, R.; Stratmann, R. E.; Yazyev, O.; Austin, A. J.; Cammi, R.; Pomelli, C.; Ochterski, J. W.; Martin, R. L.; Morokuma, K.; Zakrzewski, V. G.; Voth, G. A.; Salvador, P.; Dannenberg, J. J.; Dapprich, S.; Daniels, A. D.; Farkas, Ö.; Foresman, J. B.; Ortiz, J. V.; Cioslowski, J.; Fox, D. J. Gaussian 09, Revision E.01. Wallingford CT **2009**.